RSC Advances

PAPER

View Article Online
View Journal | View Issue

Cite this: *RSC Adv.*, 2023, **13**, 25508

Human blood-labyrinth barrier on a chip: a unique *in vitro* tool for investigation of BLB properties†

Marijana Sekulic, *[a] Narjes Abdollahi,[a] Lukas Graf,[b] Nikolaus Deigendesch,[c] Raoul Puche,[a] Daniel Bodmer[ab] and Vesna Petkovic [a]

Hearing loss is one of the leading causes of disability worldwide, usually as a result of hair cell damage in the inner ear due to aging, acoustic trauma, or exposure to antibiotics or chemotherapy. No drug therapies can protect or restore hearing and current *in vitro* and animal models used in drug discovery have a very low success rate, mostly due to major differences in anatomy and accessibility of the inner ear environment between species. The blood-labyrinth barrier (BLB) in the stria vascularis is a highly specialized capillary network that controls exchanges between the blood and interstitial space in the cochlea. The BLB is critical for normal hearing, functioning as a physical, transport, and metabolic barrier. To address its complexity and accessibility, we created the first micro-engineered human model of BLB on a chip using autogenous progenitor cells from adult temporal bones. We successfully isolated the BLB from post-mortem human tissue and established an endothelial cell and pericyte culture system on a BLB chip. Using biocompatible materials, we fabricated sustainable two chamber chips. We validated the size-dependent permeability limits of our BLB model by measuring the permeability to daptomycin (molecular weight 1.6 kDa) and midazolam (molecular weight 325.78 Da). Daptomycin did not pass through the BLB layer, whereas midazolam readily passed through the BLB in our system. Thus, our BLB-chip mimicked the integrity and permeability of human stria vascularis capillaries. This represents a major step towards establishing a reliable model for the development of hearing loss treatments.

Received 13th July 2023
Accepted 14th August 2023

DOI: 10.1039/d3ra04704k

rsc.li/rsc-advances

Introduction

Hearing loss affects more than 5% of people worldwide, yet no current drug therapies can protect or restore hearing. Pharmaceutical drugs, such as chemotherapy and antibiotic therapy, present ototoxic side effects, negatively affecting hearing. In addition, noise and age have a negative effect on hearing.[1] The inaccessible location of the inner ear within the cochlea makes drug delivery challenging in the treatment of inner ear disorders. Drug delivery cannot be studied in existing mouse organ of Corti explant culture systems, and it is difficult to monitor *in vivo*. Furthermore, because of species differences in physiology and protein expression, >80% of drug candidates that have shown promise in animal models have failed in clinical trials.[2,3] Thus, the development of therapy for hearing loss is difficult and requires better tools.

The inner ear vasculature as a point of non-invasive drug delivery is appealing, though the blood-labyrinth barrier (BLB) at the luminal surface of inner ear capillaries restricts the entry of most blood-borne compounds into inner ear tissues.[4] The stria vascularis is a highly vascularized tissue in the lateral wall of the cochlea that is essential for generating and maintaining the unique ionic composition of the endolymph in the scala media. The inner ear is a remarkably stable homeostatic system controlled by a range of regulatory mechanisms, including control over ions, fluid, and nutrient transport (active and passive) by the BLB. The BLB between the systemic circulation and stria vascularis is crucial for maintaining cochlear and vestibular homeostasis, facilitating nutrient and metabolite transport into the cochlea, and protecting the cochlea against inflammation and disease. Strial capillaries are non-fenestrated with tight junctions between adjacent endothelial cells (ECs), forming a BLB that separates intrastrial fluids from the blood. The BLB is comprised of ECs, pericytes (PCs), and perivascular-resident macrophage-like melanocytes (PVM/Ms), which are essential for maintaining barrier integrity (Fig. 1a).[5] Within the stria vascularis, there are also marginal and basal cells that build a continuous layer of cells connected by complexes of narrow joints. Between these cellular structures is an intrastrial space with a BLB. The physiological significance of marginal cells is not known.[6] Interactions between ECs and PCs are critical for controlling vascular integrity and permeability and for providing an optimal microenvironment for hearing.

[a]*Department of Biomedicine, University Hospital Basel, University of Basel, Basel, Switzerland. E-mail: marijana.sekulic@unibas.ch*

[b]*Clinic for Otolaryngology, Head and Neck Surgery, University Hospital Basel, Basel, Switzerland*

[c]*Institute of Pathology, University Hospital Basel, Switzerland*

† Electronic supplementary information (ESI) available. See DOI: https://doi.org/10.1039/d3ra04704k

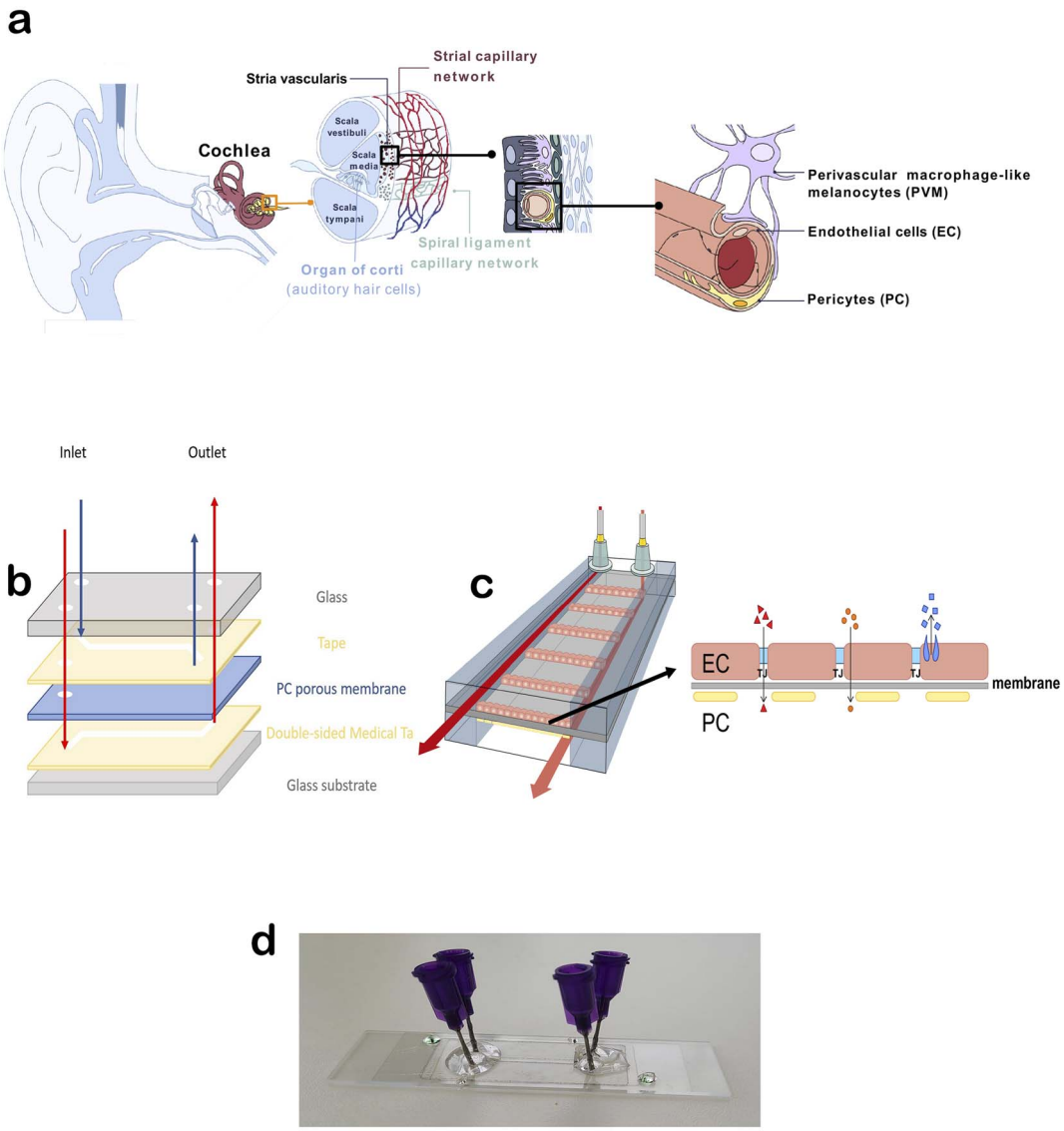

Fig. 1 (a) Schematic of the cochlea and subsequent elements depicting the localization of the stria vascularis and blood vessels with the blood-labyrinth barrier and its component cells. (b) Schematics of the chip and its main components and materials and (c) the assembled chip with endothelial cells and pericytes positioned on the membrane with tight junctions (TJ) that form a selectively permeable barrier, which is the rate-limiting step of paracellular transport (red triangles). A few examples of other forms of transport across the BLB are shown in orange circles (osmosis) and blue squares (receptor-mediated transport). (d) Final image of the assembled chip used for permeability testing.

The physiological function of the BLB is to respond to the special needs of the inner ear, including nutrient supply, ion absorption, waste excretion, protection from toxins, and fluid filtration. The BLB is still not fully understood, making drug development for inner ear diseases difficult. In addition, quantification of the barrier's permeability of is necessary to assess its condition and identify factors that contribute to barrier dysfunction. Monitoring barrier integrity allows assessment of the toxic effects of compounds, and deregulation of the barrier's essential function can lead to serious health complications. The inner ear is often the first organ affected in systemic autoimmune diseases, probably due to mild vascular pathologies affecting the ear faster than any other organ system.[7] Malfunction of the stria vascularis and BLB can alter the electrochemical composition of the endolymph, resulting in loss of the endocochlear potential, elevated auditory thresholds, and hearing loss. BLB defects are associated with inner ear diseases that lead to hearing loss, including vascular malformations, Meniere's disease, Alport syndrome, and Pendred syndrome, as well as aging.[8–11]

Development of a model system that can facilitate drug development and delivery into the inner ear is crucial. In recent years, several new technologies have emerged to improve *in vitro* models of the blood–brain barrier (BBB) for drug testing, such as the Transwell model, microfluidic chip/membrane model, microfluidic parallel channel models, and templated model.[12] On the other hand, no similar models of the BLB have been described. To study the transport of drugs through human stria

vascularis, an adequate model needs to be developed. Our aim was to develop the first human BLB dynamic model for use in drug testing for hearing loss. For the first time, we have isolated human stria vascularis-derived ECs and PCs and placed them in a dynamic chip system made in our lab to recreate the human BLB. We confirmed cell growth within the system and validated the barrier integrity and permeability. These results will allow further fine-tuning and optimization to standardize the chip platform for BLB studies and offer a promising high-throughput approach for preclinical screening of innovative therapies that target specific BLB transporters and permeability. This technology will be the best *in vitro* option available to date for inner ear drug testing.

Experimental

BLB chip fabrication

The overall blueprint of the chip was modified from Winkler *et al.*[13] We initially started with two double-coated pressure-sensitive adhesives for fabrication of our chip; polyethylene tape with tackified acrylic-based adhesive (No. 9889) and polyester white tape with acrylic-based adhesive (No. 9965), both provided by 3 M (3 M Central Europe Region, Germany). After testing as described in the results below, we opted for the polyethylene tape. A porous transparent polycarbonate membrane 25 μm-thick with a pore size of 0.4 μ and pore density of 1.60° ϕ 106 pores per cm^2 (ipCELLCULTURE Track Etched Membrane, supplied by it4ip, Belgium) was used. The top and bottom channel designs were patterned on the adhesives and membrane using a laser cutter (Flux Beambox, Taiwan). The channels had a height of approximately 120 μm and width of 1.5 mm. Glass slides with thicknesses of 1 mm and 130–170 μm were used as the top and bottom covers, respectively. For the top cover, the holes for inlets and outlets were drilled manually. The sandwich-style BLB chip was built up under an optical microscope for precise alignment of the layers, and a bench vice was used to bind the layers. Blunt-end luer lock syringe needles (21 G, Darwin Microfluidics) were used as the inlet and outlet connections and glued to the chip with Araldite crystal glue.

Tissue isolation and cell culture

We established a protocol for the isolation, maintenance, and differentiation of human stria vascularis from human post-mortem tissues obtained from the Pathology Institute in Basel Switzerland (Ethical permit: EKNZ 2020-01379). Autopsy-derived post-mortem human temporal bones were used as a tissue source for the present study due to the paucity of surgical procedures in which healthy stria vascularis tissue could be obtained. All patients or their relatives provided informed consent for the use of autopsy material for scientific purposes. Donors were from both genders and ranges in age from 50 to 75 years. Exclusion criteria were prior hearing disorders or loss, recent chemotherapy, and any diseases that could affect hearing. The samples were collected an average 11 h, but up to 18 h, post-mortem. During autopsy, the skulls were opened as usual by removing the skull cap. After removal of the brain, the dura mater at the base of the skull was pulled off. The petrous part of the temporal bone was removed from the base of the skull en bloc using an oscillating saw, so that the middle and inner ear were not opened during removal. The excised bone fragment was immersed in 70% (v/v) ethanol for 30 s and subsequently placed in sterile PBS containing penicillin/streptomycin (100 U ml^{-1}) and stored at 4 °C until further processing. The temporal bone specimens were stabilized in a temporal bone holder (Storz & Co., Tuttlingen, Germany). An open tympanoplasty approach was performed. After a subtotal mastoidectomy, the superior and posterior canal wall, tympanic membrane, malleus, and incus were removed. The protympanon was enlarged to the petrous segment of the internal carotid artery. Parts of the tympanic segment of the facial nerve and tendon of the *m. tensor tympani* were dissected to access the full circumference of the cochlea. The promontory bone was blue-lined with a diamond drill until the cochlear turns were visible. The lateral bone of the turns was completely drilled away and the membranous labyrinth of the cochlea carefully extracted. Tissue was trypsinized with Trypsin–EDTA 0.25% (Sigma cat# T4049) for 5 min, and then blocking solution with 10% FBS was added, followed by centrifugation at 1500 rpm for 5 min. Tissue pieces were distributed in wells coated with 0.03 mg ml^{-1} fibronectin in DPBS (ScienCell cat# 8248) or 0.01 mg ml^{-1} poly-L-lysine in sterile water (ScienCell cat# 0403) to seed ECs and PCs, respectively, and then rinsed with sterile water and DPBS. The cells were seeded and incubated at 37 °C in 5% CO_2. The medium was changed every 2 days. The growth medium for ECs consisted of 500 ml EC basal medium, 25 ml FBS (ScienCell cat# 0025), 5 ml EC growth supplement (ScienCell cat# 1052), and 5 ml penicillin/streptomycin solution (ScienCell cat# 0503). The PC growth medium consisted of 500 ml PC basal medium, 10 ml FBS (ScienCell cat# 0010), 5 ml PC growth supplement (ScienCell cat# 1252), and 5 ml penicillin/streptomycin solution (ScienCell cat# 0503). Before placing the cells in the chip, the cell type was validated at the gene and protein level using immunostaining and gene expression of marker proteins described below.

Real-time PCR

RNA was isolated from cells collected from a confluent T-75 flask (Thermo Fisher, cat# 156499) and extracted using the Direct-Zol RNA MiniPrep kit (Zymo Research, Germany, cat# R2050) according to the manufacturer's instructions. Total RNA (1000 ng) was reverse transcribed using a High-Capacity cDNA Reverse Transcription Kit (Applied Biosystems, United States). We analysed triplicate samples by quantitative PCR on an ABI Prism 7900HT Sequence Detection System (Applied Biosystems, United States) using the Power Sybr Green Master Mix (Applied Biosystems, United States). Primers targeting the *vWf*, *Slc2a1*, *Cd34*, *Des*, *Pdgfrb*, *Cspg4*, and *Gapdh* genes were synthesized by Microsynth (St. Gallen, Switzerland) and added at a final concentration of 250 nM per reaction. The full primer sequences used in this study are as follows (5′–3′): *vWf*: Fw-AGCCTTGTGAAACTGAAGCAT, Rev-TCCCCAAGATACACGGAGAGG; *Slc2a1*: Fw-

GGCCAAGAGTGTGCTAAAGAA, Rev-ACAGCGTTGATGCCAGACAG; *Cd34*: Fw-CTACAACACCTAGTACCCTTGGA, Rev-GGTGAACACTGTGCTGATTACA; *Des*: Fw-TCGGCTCTAAGGGCTCCTC, Rev-CGTGGTCAGAAACTCCTGGTT; *Pdgfrb*: Fw-AGCACCTTCGTTCTGACCTG, Rev-TATTCTCCCGTGTCTAGCCCA; *Cspg4*: Fw-CTTTGACCCTGACTATGTTGGC, Rev-TGCAGGCGTCCAGAGTAGA; *Gapdh*: Fw-GGAGCGAGATCCCTCCAAAAT, Rev-GGCTGTTGTCATACTTCTCATGG. The relative quantities of specifically amplified cDNAs were calculated by the comparative threshold cycle method, and Gapdh expression was used as the endogenous reference.

Immunostaining and imaging

Test samples of each cell phenotype were grown on 4-well collagen-coated glass-bottom dishes (Ibidi, Germany, cat# 80426). Cells were fixed in 4% paraformaldehyde (Sigma, United States, cat# 158127) in PBS (Sigma, United States, cat# P4417), permeabilized with 0.1% Triton X-100 (Sigma, United States, cat# X100) in PBS, and incubated for 1 h at room temperature with anti-von Willebrand factor (*vWf*, Sigma, United States, cat# F3520) and anti-PDGFR-β (Santa Cruz Biotechnology, United States, cat# sc374573) primary antibodies. Next, samples were washed and incubated with appropriate secondary antibodies (Thermo Fisher, United States, cat# A2124, cat# A-11001, cat# A-11008) in PBS-T for 1 h at room temperature. Samples were washed with PBS and incubated with DAPI for 5 min. The cells were washed with PBS and mounted on microscope slides using Dako Fluorescent Mounting medium (Dako, Denmark, cat# S3023). Images were captured by a Nikon Eclipse Ti2 inverted widefield microscope.

Transepithelial electrical resistance (TEER)

Transepithelial electrical resistance (TEER) was measured with a Voltohmmeter EVOM3. For TEER measurements, ECs were seeded at a density of 2×10^5 cm^{-2} and grown on membrane inserts (Corning, cat# 3470) coated with fibronectin. The PCs were combined with ECs (harvested after 2 and 3 passages and seeded at a density of 110^5 cm^{-2}) and grown on the poly-L-lysin-coated inserts. The measurements were obtained following the manufacturer's protocol. Briefly, electrodes were maintained by soaking the tips once a week in a 1% Tergazyme solution for 15 minutes and rinsing with sterile water, and the same was done just before disinfection and before beginning an experiment. The STX4 electrode were disinfected in 70% ethanol for no more than 5 minutes, followed by rinsing with medium or PBS. This was followed by measuring the resistance in test samples containing cells and blank without cells.

After finishing the measurement, electrodes were disinfected with ethanol and rinsed with sterile water and allowed to air dry. To calculate TEER, the surface area of the Transwell (in cm^2) was multiplied by the net resistance (the resistance of a blank Transwell covered by cell culture media subtracted from the measured resistance).

Seeding cells on the BLB chip

Initially, the chip was sterilized by perfusion of ethanol (70 wt%) at a flow rate of 15 μl min^{-1} and then rinsed with PBS. The bottom channel was treated with rat tail collagen (rinsed with PBS) and poly-L-lysine (0.01 mg ml^{-1}) in sterile water (rinsed with sterile water). The top channel was treated with rat tail collagen (rinsed with PBS) and fibronectin (0.03 mg ml^{-1}) in DPBS (rinsed with DPBS). The channels were then rinsed with the appropriate EC or PC medium.

The PCs were trypsinized and detached from the culture flask and centrifuged for 5 min at 1100 rpm. The cell pellet was then suspended in cell medium. After counting the cells using Trypan Blue in the automated cell counter (Bio-Rad, TC20) PCs were injected into the bottom chamber by syringe, approximately 200 000 cells per injection. After 3 h incubation, the chip was flipped onto its other side and the ECs introduced into the top channel. The chip was cultured in static mode for 2–3 days. The development of cells inside the BLB chip was monitored using an inverted light microscope with a magnification of 10×. After successful validation of the growth and development of cells within the chip, the BLB chip was connected to a peristaltic pump for medium perfusion (dynamic mode) at a flow rate of 5 μl min^{-1}. We used Ismaprene PharMed 2-stop tubing with an inner diameter of 0.25 mm (SC0320, supplied by MasterFlex) for the peristaltic pump. Ismaprene PharMed standard tubing with an inner and outer diameter of 1.6 mm and 4.8 mm, respectively (MF0010, supplied by MasterFlex), was used for connections. A 16-channel IPC digital peristaltic pump (Ismatec) was used for the perfusion of fluids into the chip. The tubes were sterilized with ethanol, and then rinsed with PBS before being used for medium perfusion. The medium was changed every 2 days.

Permeability assay

Autoclaved 15 ml centrifuge tubes (Corning, cat# CLS430791) with holes in the cap were used as inlet and outlet reservoirs. To the EC medium for the top channel, 10 μg daptomycin (Sigma, cat# SBR00014) or 1 μg midazolam (LGC Standards, cat# LGCFOR1106.00) was added to test the permeability, whereas the basolateral bottom channel was perfused with PC medium. The BLB chip and reservoirs were then connected to the pump with the flow rate set at 5 μl ml^{-1}. The chip with no cells was used as a control sample and prepared the same way as the chip with cells attached. The dead volumes of tubes and purple connectors were calculated by considering flow rate (5 μl ml^{-1}), and the first sample from the outlet reservoirs was taken at $T =$ 0 min. A 20 μl aliquot was taken from the apical and basolateral chamber outlet reservoirs at defined time points for both the BLB chip with cells and control sample: 30 min, 1.5 h, 3 h, 6 h, and 24 h. The samples were then evaluated by HPLC to determine their concentrations.

HPLC

HPLC analysis was performed on an ultrahigh-performance liquid chromatography system from Shimadzu (Kyoto, Japan), which was coupled to an API 5500 QTrap tandem mass

spectrometer (AB Sciex, Framingham, MA, USA). Analytes were separated on a pentafluorophenyl core shell (Kinetex 2.6 μm F5 100 Å, 50 × 2.1 mm) analytical column (Phenomenex, Torrance, USA). Mobile phase A consisted of water with 0.01% acetic acid. Mobile phase B was methanol. The column was conditioned with 2% mobile phase B during the first 0.25 min of the analytical run. Afterwards, the mobile phase B concentration was linearly increased to 95% over 2.75 min and kept at this level for another 0.75 min. Finally, the column was reconditioned at 2% mobile phase B for 0.25 min. The flow rate was set to 0.6 ml min^{-1} and the column oven at 50 °C. The injected sample was diluted with mobile phase A through a tee union in a ratio of 1 : 10 during the first 0.25 min of each run. The analytes were ionized in an electrospray source and detected by multiple reaction monitoring in the positive and negative mode. Nitrogen was used as the ion source, curtain, and collision gas. The ion spray voltage was set at 5500 V (positive mode) and 4500 V (negative mode). The source temperature was set to 500 °C. The LC-MS/MS system was operated using Analyst software 1.6.2 (AB Sciex, Framingham, MA, USA).[14]

Statistical analysis

Statistical analyses were performed in GraphPad Prism software (San Diego, CA, United States). Multiple groups were compared by two-way analysis of variance, and two groups were compared

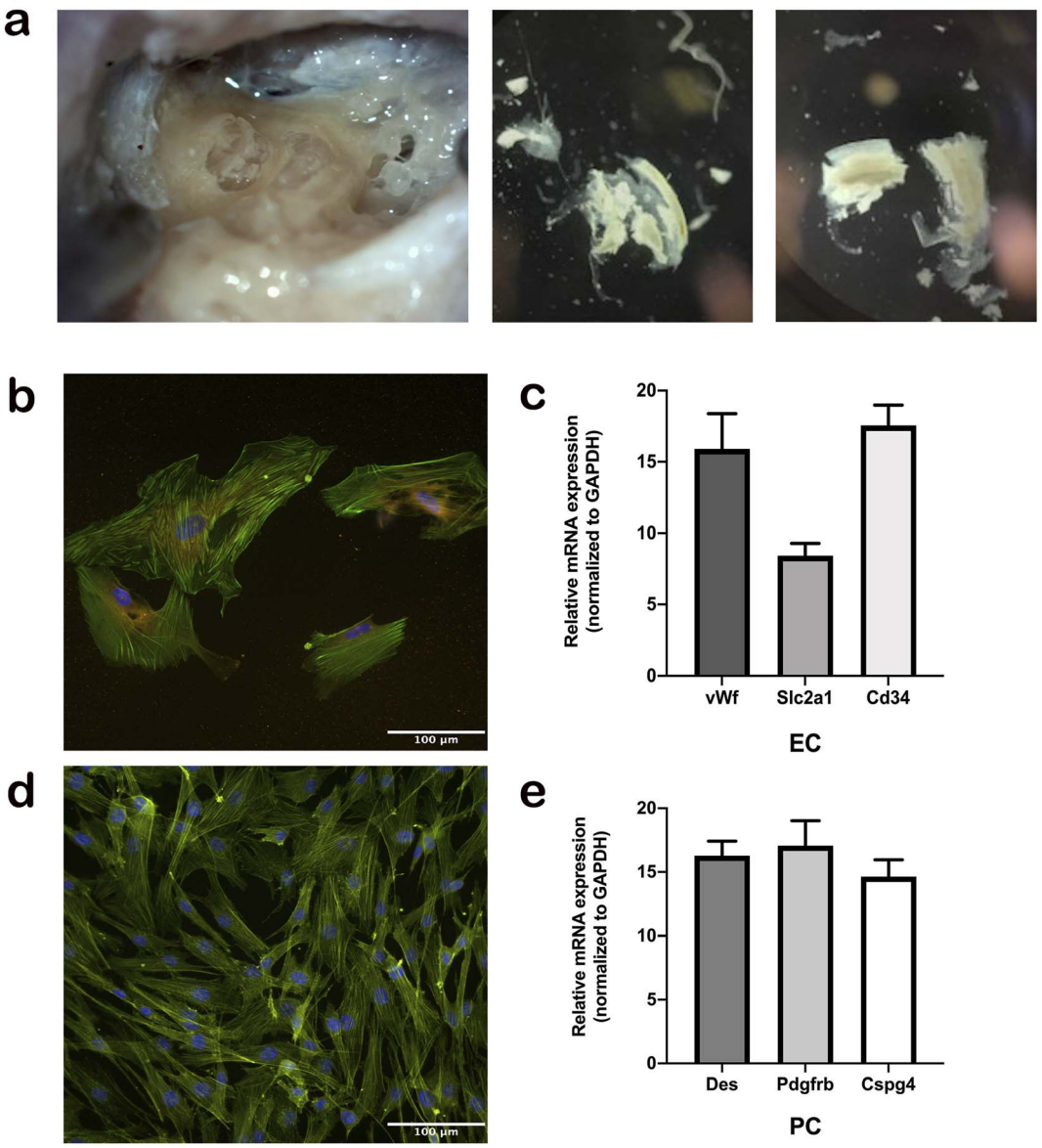

Fig. 2 (a) Image of the human temporal bone taken during stria vascularis isolation. The cochlea is in the centre left part of the first image and pieces of isolated stria vascularis in the other two images. (b) Fluorescently labelled images of the endothelial cells stained with endothelial marker von willebrand factor in red, phalloidin in green, and DAPI in blue. (c) Cell specificity was confirmed by the gene expression of several major markers of endothelial cells: *vWf*, *slc2a1*, and *Cd34*. (d) Immunostaining of pericytes with PDGFR-β marker and DAPI. (e) Cell phenotype was confirmed using specific marker genes for pericytes: *Des*, *Pdgfrb*, and *Cspg4*.

by an unpaired Student's *t*-test. Data were confirmed to be normally distributed by a Shapiro–Wilk test. *P*-values < 0.05 were considered significant.

Results

Microfluidic device assembly

The initial design of the chip was modified from the literature as shown in Fig. 1b.[13] The primary idea was to have ECs on one side of the porous membrane and PCs on the other side to recreate the BLB environment (Fig. 1c). We first tested the glass bottom and PDMS cover with medical tape connecting them. As this was prone to leakage in our setup, we opted for glass covers on the top and bottom. We initially started with two double-coated pressure-sensitive adhesives for fabrication of our chip: polyethylene tape with tackified acrylic-based adhesive and polyester white tape with acrylic-based adhesive. After performing several leakage tests, the most durable configuration was a combination of polyethylene tape and glass. A porous transparent polycarbonate membrane (thickness 25 μm, pore size 0.4 μ, pore density 1.60° ϕ 106 pores per cm^2) was used as the barrier. The top and bottom channel designs were patterned on the adhesives and membrane using a laser cutter. The channels had a height of approximately 120 μm and width of 1.5 mm. Glass slides with thicknesses of 1 mm and 130–170 μm were used as the top and bottom covers, respectively. For the top cover, the holes for inlets and outlets were drilled manually. The sandwich-style BLB chip was built up under an optical microscope for precise alignment of the layers, and a bench vice was used to bind the layers. Blunt-end luer lock syringe needles were used as the inlet and outlet connections and glued to the chip with Araldite crystal glue (Fig. 1d).

Human stria vascularis-derived primary EC and PC cultures

For the first time, we established a protocol for the isolation, maintenance, and differentiation of human stria vascularis cells from human post-mortem temporal bone samples (Fig. 2a). After the third passage from the initial tissue sample, cells were immuno-stained with appropriate markers of cell phenotype. Human ECs were stained with *vWf* antibody (Fig. 2b) and human PCs with *Pdgfrb* antibody (Fig. 2d), and both cell culture types were confirmed to be populated with ≥90% of the appropriate phenotype. In later subculturing steps, the cell cultures became even more uniform. In addition, we performed gene expression assays regularly to ensure the phenotype remained consistent for both cell types throughout the process (Fig. 2a and c).

Growth of human-derived ECs and PCs in a microfluidic device

After phenotype confirmation, the cells were seeded on the chip 200 000 ECs per injection in the fibronectin-coated top channel and 200 000 PCs in the poly-L-lysin-coated bottom channel. After successful validation of the growth and development of cells within the chip (Fig. 3a and b), which usually occurred around day 2–3 post-seeding, the chip was connected to the peristaltic pump containing appropriate growth media for each cell type. We used a flow rate of 5 μl min^{-1}, which corresponds to the blood flow levels in the cochlea. The exact limit on cell

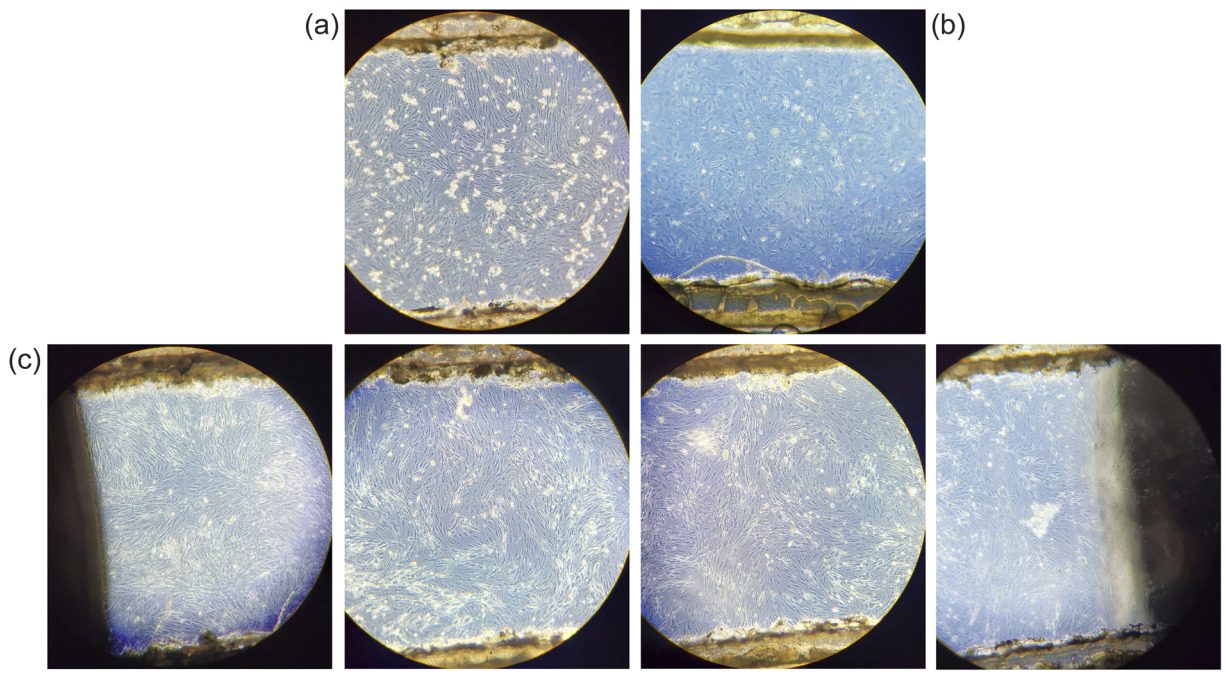

Fig. 3 (a) Endothelial cells and (b) pericytes after seeding on a chip. (c) Images of the top channel 6 days after seeding endothelial cells. Endothelial cells were evenly distributed on the chip membrane along the channel length from the inlet towards the outlet after being connected to the peristaltic pump.

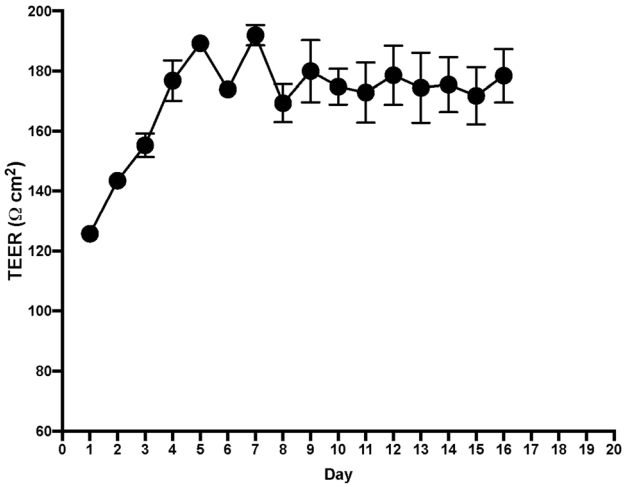

Fig. 4 TEER measurement values after seeding endothelial cells and pericytes on a transwell insert with polyester membrane. Stable values were reached at day 7, which indicates good integrity of the barrier on the transwell.

maintenance in the chip is yet to be determined, but we established long-term maintenance of cells up to 24 days (Fig. 3c). To confirm maintenance of the cell phenotype on the chip, cells were stained after 3 weeks with their appropriate markers and imaged (ESI Fig. S1†).

TEER and permeability validated in human-derived BLB system

After measuring TEER in the EC layer, we found stable TEER levels 7 days after seeding the cultures, with continuing steady levels through the next 10 days (Fig. 4). Following these results, we tested permeability on the BLB chip using known compounds. A functional BLB model should guarantee selective permeability to molecules based on their molecular weight. We used daptomycin, which has a molecular weight of 1619 Da, greater than the BLB permeability limit, and midazolam, which has a molecular weight of 325.78 Da, below the BLB permeability limit. Samples were collected for HPLC at 30 min, 1 h, 1.5 h, 2 h, 3 h, 4 h, and 24 h. For 10 μg daptomycin, we detected no daptomycin in the channel with PCs compared with the control channel with no cells where the influx of daptomycin was unrestricted (Fig. 5a). In contrast, for 1 μg midazolam placed in the channel with ECs, we detected similar levels of daptomycin in the bottom channel regardless of the presence or absence of the cells in the chip (Fig. 5b). Thus, the BLB cell barrier created in our chip model is not permeable to substances above the BLB permeability threshold. Therefore, at least in this aspect, the model behaves similarly to the barrier found in physiological conditions.

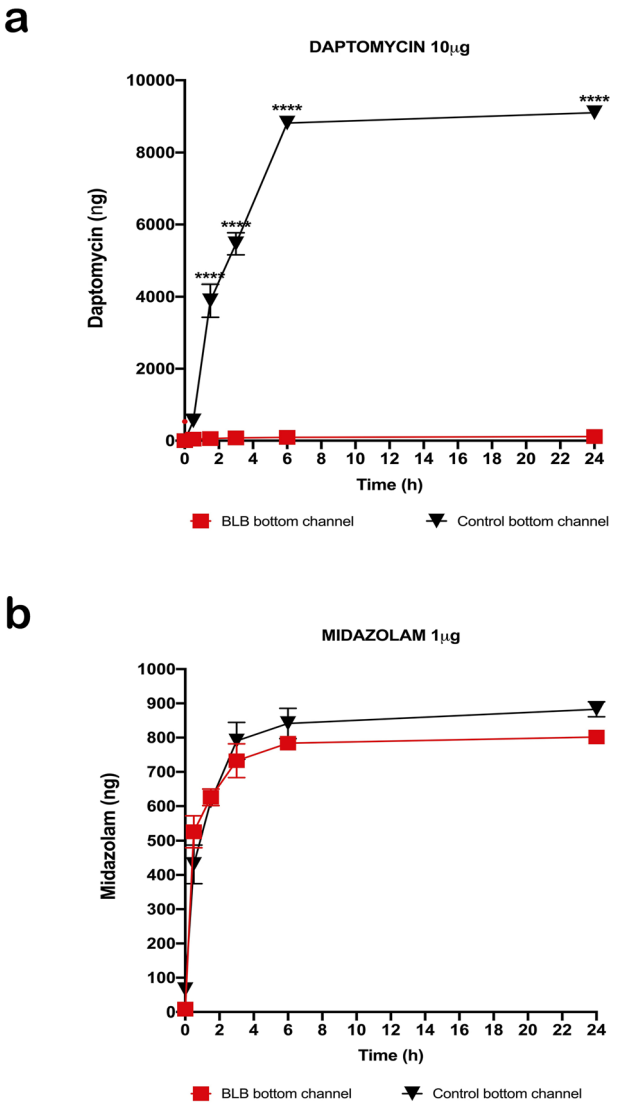

Fig. 5 Permeability values after HPLC analysis of the samples collected from the basolateral channel. An aliquot (20 μl) was taken from the apical and basolateral channel outlet reservoirs of both the BLB chip with cells and control sample at defined time points: 30 min, 1.5 h, 3 h, 6 h, and 24 h (for the simplicity of interpretation, we are showing only results for the concentrations found in the basolateral channel outlet reservoirs). The dead volumes of tubes and purple connectors were calculated during sample collection. (a) For 10 μg daptomycin, we detected no daptomycin in the channel with pericytes compared to control with no cells for which the influx of daptomycin was unrestricted. For time points 30 min, 1.5 h, 3 h, 6 h. and 24 h there was a significant difference in permeability between the chip with cells and the chip with no cells (****$p < 0.0001$, $n = 6$). (b) For 1 μg midazolam placed in the apical channel with endothelial cells, we detected similar levels as daptomycin in the basolateral channel regardless of the presence or absence of the cells in the chip. We found no significant difference between the results (n.s., $n = 6$). Data are presented as mean ± SD.

Discussion

The high selectivity of the BLB has hampered the therapeutic treatment of inner ear diseases and hearing loss overall.[4,15] The exact physiological function of the human BLB has not yet been explored, and the requirements for drug entry across the BLB have not been described. Recent progress in Transwell cell culture systems and organ-on-chip technology has provided useful insights into the largely unknown and poorly understood

mechanisms involved in BBB physiology.[16] The BLB is analogous to the BBB because it allows the passage of select molecules into labyrinthal spaces. Mechanisms enabling the trafficking of therapeutics across the BLB are conceptually similar to those for the BBB but require specialized adaptations specific to the cochlea and vestibular system.[17] In addition, inappropriate *in vivo* and *in vitro* models have led to the requirement of a novel *in vitro* BLB model. Static models, such as Transwell, are used for various tissues, including the BBB, and can be a good initial step into further testing.[18,19] The major drawback of a static system when modelling a blood vessel environment is lack of flow, which creates sheer stress and promotes EC growth and the creation of a tight barrier while preventing their dedifferentiation.[20,21] For these reasons dynamic organ-on-a-chip has been employed to better recapitulate the human *in vivo* microenvironment to facilitate the prediction of drug responses. Many disease modelling and transport mechanism studies have been implemented using BBB-on-a-chip, whereas BLB models are completely absent.[22–25]

Here, for the first time, we showed that a human BLB model can be established, representing a critical point in the future of drug discovery and validation in hearing loss treatment. One of the major challenges for any study of this type is access to human tissue and the ability to gain progenitor cells. Using post-mortem tissue is not the most favourable option, but due to the inner ear's inaccessibility, it is practically one of the only options available for obtaining human tissue and recapitulating the environment within the human BLB as closely as possible. In this study, we have successfully isolated and placed on a chip two major cell types, endothelial cells and pericytes, that are budling a barrier between the blood and intrastrial space. Further challenges in developing this model will include addling compartments that mimic endolymph and intrastrial fluid lined with marginal, intermediate and basal cells. Primary cells are superior to immortalized cell lines when it comes to replicating the functional and physiological aspects of the human BLB because they have normal cell morphology and maintain many of the important markers and functions seen *in vivo*, whereas EC lines lack various functional markers.[26–29] For these reasons, even if primary cells are more difficult to work with, the data obtained from using primary cells is more relevant and reflective of the *in vivo* environment.

Choosing the optimal materials for the chip design and its purpose is often challenging. To date, many substrates have been used to manufacture microfluidic chips, including silicon, polydimethylsiloxane (PDMS), polymethyl methacrylate (PMMA), and glass.[30–33] Silicon has good chemical and thermal stability, but also has a relatively high cost, opacity, and complex surface chemical properties that make it difficult to integrate into cell-based chips. On the other hand, PDMS and PMMA are widely used in biochips in both academic and industrial fields due to their high efficiency and low fabrication cost. PDMS serves as a good option for academic research, but when it comes to testing various drug candidates, its ability to adsorb hydrophobic molecules or, when stable surface characteristics are required, issues of dissolution and surface property control pose a problem.[34–36] In addition, it is not ideal material for cell growth and attachment under sheer stress conditions. To optimize the testing conditions for all kinds of compounds, we chose glass instead of PDMS. Glass has proven to be a more suitable substrate for microfluidic chips. It has high surface stability, great optical transparency, biocompatibility, is chemically inert, and can be efficiently coated.[37,38] Another important aspect of chip fabrication is assembly. When there is a membrane involved, the most usual combination is glass, PDMS, and thermoplastics.[39] The bonding of glass to PDMS needs to be facilitated by external means (plasma), which requires additional equipment and increases the time and costs of chip manufacturing. For these reasons, we opted for a double-coated pressure-sensitive adhesive tape, a very affordable material that can be patterned at minimal cost.

Conclusions

Our BLB organ-on-a-chip successfully recreates the structure and behaviour of the human BLB and is a substantial step forward for modelling the human BLB. This unique microfluidic device provides an environment for all cell types involved in BLB formation and the shear forces necessary for barrier formation. This device also enables evaluation of the drug effects on the endothelial function in the context of the BLB to account for drug permeability and effects on the BLB itself. Taken together, these innovations provide a novel platform for modelling human BLB function and testing drug toxicity and permeability with regard to hearing. In future studies, we aim to further standardize this system and automate some of the critical steps, as well as integrate sensors that would facilitate data collection and analysis.

Conflicts of interest

The authors have no conflicts of interest to declare.

Acknowledgements

This study was financed by Innosuisse grant (46201.1IP-LS) and Freiwillige Akademische Gesellschaft (FAG). We would like to thank Prof. Alexandar Tzankov for enabling us to obtain human post-mortem samples and PD Dr Christof Stieger for generously lending us his lab space and equipment for tissue extraction from the temporal bone. We appreciate the insights and expertise provided by PD Dr Urs Duthaler when doing HPLC. Finally, we would like to thank Radmila Trajanoska for her contribution to technical work and laboratory maintenance.

References

1 L. L. Cunningham and D. L. Tucci, Hearing Loss in Adults, *N. Engl. J. Med.*, 2017, **377**, 2465–2473, DOI: **10.1056/NEJMra1616601**.

2 A. Akhtar, The flaws and human harms of animal experimentation, *Camb. Q Healthc. Ethics*, 2015, **24**, 407–419, DOI: **10.1017/s0963180115000079**.

3 R. Greek, A. Menache and M. J. Rice, Animal models in an age of personalized medicine, *Pers. Med.*, 2012, **9**, 47–64, DOI: **10.2217/pme.11.89**.

4 S. Nyberg, N. J. Abbott, X. Shi, P. S. Steyger and A. Dabdoub, Delivery of therapeutics to the inner ear: The challenge of the blood-labyrinth barrier, *Sci. Transl. Med.*, 2019, **11**(482), eaao0935, DOI: **10.1126/scitranslmed.aao0935**.

5 L. Neng, F. Zhang, A. Kachelmeier and X. Shi, Endothelial cell, pericyte, and perivascular resident macrophage-type melanocyte interactions regulate cochlear intrastrial fluid-blood barrier permeability, *J. Assoc. Res. Otolaryngol.*, 2013, **14**, 175–185, DOI: **10.1007/s10162-012-0365-9**.

6 D. C. Marcus, in *Cell Physiology Source Book*, ed N. Sperelakis, Academic Press, 4th edn, 2012, pp. 649–668.

7 A. F. Goodall and M. A. Siddiq, Current understanding of the pathogenesis of autoimmune inner ear disease: a review, *Clin. Otolaryngol.*, 2015, **40**, 412–419, DOI: **10.1111/coa.12432**.

8 S. Gu, et al., Identification of Potential Meniere's Disease Targets in the Adult Stria Vascularis, *Front. Neurol.*, 2021, **12**, 630561, DOI: **10.3389/fneur.2021.630561**.

9 P. Wangemann, et al., Loss of KCNJ10 protein expression abolishes endocochlear potential and causes deafness in Pendred syndrome mouse model, *BMC Med.*, 2004, **2**, 30, DOI: **10.1186/1741-7015-2-30**.

10 M. A. Gratton, V. H. Rao, D. T. Meehan, C. Askew and D. Cosgrove, Matrix metalloproteinase dysregulation in the stria vascularis of mice with Alport syndrome: implications for capillary basement membrane pathology, *Am. J. Pathol.*, 2005, **166**, 1465–1474, DOI: **10.1016/s0002-9440(10)62363-2**.

11 A. Heeringa and C. Köppl, The aging cochlea: Towards unraveling the functional contributions of strial dysfunction and synaptopathy, *Hear. Res.*, 2019, **376**, 111–124, DOI: **10.1016/j.heares.2019.02.015**.

12 R. M. Linville and P. C. Searson, Next-generation in vitro blood–brain barrier models: benchmarking and improving model accuracy, *Fluids Barriers CNS*, 2021, **18**, 56, DOI: **10.1186/s12987-021-00291-y**.

13 T. E. Winkler, M. Feil, E. F. G. J. Stronkman, I. Matthiesen and A. Herland, Low-cost microphysiological systems: feasibility study of a tape-based barrier-on-chip for small intestine modeling, *Lab Chip*, 2020, **20**, 1212–1226, DOI: **10.1039/D0LC00009D**.

14 C. Suenderhauf, et al., Pharmacokinetics and phenotyping properties of the Basel phenotyping cocktail combination capsule in healthy male adults, *Br. J. Clin. Pharmacol.*, 2020, **86**, 352–361, DOI: **10.1111/bcp.14157**.

15 X. Shi, Pathophysiology of the cochlear intrastrial fluid-blood barrier (review), *Hear. Res.*, 2016, **338**, 52–63, DOI: **10.1016/j.heares.2016.01.010**.

16 D. Huh, et al., Microfabrication of human organs-on-chips, *Nat. Protoc.*, 2013, **8**, 2135–2157, DOI: **10.1038/nprot.2013.137**.

17 D. T. Phan, et al., Blood–brain barrier-on-a-chip: Microphysiological systems that capture the complexity of the blood-central nervous system interface, *Exp. Biol. Med.*, 2017, **242**, 1669–1678, DOI: **10.1177/1535370217694100**.

18 N. L. Stone, T. J. England and S. E. O'Sullivan, A Novel Transwell Blood–Brain Barrier Model Using Primary Human Cells, *Front. Cell. Neurosci.*, 2019, **13**, DOI: **10.3389/fncel.2019.00230**.

19 J. J. Jamieson, P. C. Searson and S. Gerecht, Engineering the human blood–brain barrier in vitro, *J. Biol. Eng.*, 2017, **11**, 37, DOI: **10.1186/s13036-017-0076-1**.

20 C. F. Buchanan, S. S. Verbridge, P. P. Vlachos and M. N. Rylander, Flow shear stress regulates endothelial barrier function and expression of angiogenic factors in a 3D microfluidic tumor vascular model, *Cell Adhes. Migr.r*, 2014, **8**, 517–524, DOI: **10.4161/19336918.2014.970001**.

21 J. M. Tarbell, Shear stress and the endothelial transport barrier, *Cardiovasc. Res.*, 2010, **87**, 320–330, DOI: **10.1093/cvr/cvq146**.

22 E. Chin and E. Goh, Blood–brain barrier on a chip, *Methods Cell Biol.*, 2018, **146**, 159–182, DOI: **10.1016/bs.mcb.2018.06.003**.

23 N. R. Wevers, et al., A perfused human blood–brain barrier on-a-chip for high-throughput assessment of barrier function and antibody transport, *Fluids Barriers CNS*, 2018, **15**, 23, DOI: **10.1186/s12987-018-0108-3**.

24 S. I. Ahn, et al., Microengineered human blood–brain barrier platform for understanding nanoparticle transport mechanisms, *Nat. Commun.*, 2020, **11**, 175, DOI: **10.1038/s41467-019-13896-7**.

25 S. Lee, M. Chung and N. L. Jeon, in *The Blood–Brain Barrier: Methods and Protocols*, ed. N. Stone, Springer US, 2022, pp. 251–263.

26 C. Pan, C. Kumar, S. Bohl, U. Klingmueller and M. Mann, Comparative proteomic phenotyping of cell lines and primary cells to assess preservation of cell type-specific functions, *Mol. Cell. Proteomics*, 2009, **8**, 443–450, DOI: **10.1074/mcp.M800258-MCP200**.

27 R. Barallon, S. R. Bauer, J. Butler, A. Capes-Davis, W. G. Dirks, E. Elmore, M. Furtado, L. Kerrigan, M. C. Kline, A. Kohara, G. V. Los, R. A. F. MacLeod, J. R. W. Masters, M. Nardone, R. M. Nardone, R. W. Nims, P. J. Price, Y. A. Reid, J. Shewale, A. F. Steuer, D. R. Storts, G. Sykes, Z. Taraporewala, J. Thomson and American Type Culture Collection Standards Development Organization Workgroup ASN-0002, Cell line misidentification: the beginning of the end, *Nat. Rev. Cancer*, 2010, **10**, 441–448, DOI: **10.1038/nrc2852**.

28 E. A. Lidington, D. L. Moyes, A. M. McCormack and M. L. Rose, A comparison of primary endothelial cells and endothelial cell lines for studies of immune interactions, *Transplant Immunol.*, 1999, **7**, 239–246, DOI: **10.1016/s0966-3274(99)80008-2**.

29 L. Deng, et al., Gene expression in immortalized versus primary isolated cardiac endothelial cells, *Sci. Rep.*, 2020, **10**, 2241, DOI: **10.1038/s41598-020-59213-x**.

30 M. A. Shoffner, J. Cheng, G. E. Hvichia, L. J. Kricka and P. Wilding, Chip PCR. I. Surface passivation of microfabricated silicon-glass chips for PCR, *Nucleic Acids Res.*, 1996, **24**, 375–379, DOI: **10.1093/nar/24.2.375**.

31 L. Yu, et al., Simple, fast and high-throughput single-cell analysis on PDMS microfluidic chips, *Electrophoresis*, 2008, **29**, 5055–5060, DOI: **10.1002/elps.200800331**.

32 T.-F. Hong, et al., Rapid prototyping of PMMA microfluidic chips utilizing a CO2 laser, *Microfluid. Nanofluid.*, 2010, **9**, 1125–1133, DOI: **10.1007/s10404-010-0633-0**.

33 L.-M. Fu, W.-J. Ju, R.-J. Yang and Y.-N. Wang, Rapid prototyping of glass-based microfluidic chips utilizing two-pass defocused CO2 laser beam method, *Microfluid. Nanofluid.*, 2013, **14**, 479–487, DOI: **10.1007/s10404-012-1066-8**.

34 M. W. Toepke and D. J. Beebe, PDMS absorption of small molecules and consequences in microfluidic applications, *Lab Chip*, 2006, **6**, 1484–1486, DOI: **10.1039/b612140c**.

35 J. D. Wang, N. J. Douville, S. Takayama and M. ElSayed, Quantitative analysis of molecular absorption into PDMS microfluidic channels, *Ann. Biomed. Eng.*, 2012, **40**, 1862–1873, DOI: **10.1007/s10439-012-0562-z**.

36 I. Rodriguez, P. Spicar-Mihalic, C. L. Kuyper, G. S. Fiorini and D. T. Chiu, Rapid prototyping of glass microchannels, *Anal. Chim. Acta*, 2003, **496**, 205–215, DOI: **10.1016/S0003-2670(03)01000-6**.

37 Q. Chen, et al., A Rapid and Low-Cost Procedure for Fabrication of Glass Microfluidic Devices, *J. Microelectromech. Syst.*, 2007, **16**, 1193–1200, DOI: **10.1109/JMEMS.2007.902467**.

38 T. Wang, J. Chen, T. Zhou and L. Song, Fabricating Microstructures on Glass for Microfluidic Chips by Glass Molding Process, *Micromachines*, 2018, **9**, 269, DOI: **10.3390/mi9060269**.

39 M. W. van der Helm, A. D. van der Meer, J. C. T. Eijkel, A. van den Berg and L. I. Segerink, Microfluidic organ-on-chip technology for blood–brain barrier research, *Tissue Barriers*, 2016, **4**, e1142493, DOI: **10.1080/21688370.2016.1142493**.